Integrative Modeling of Bacterial H2O2 Stress Responses

Chen Liao

February 14, 2019

1 Background knowledge

Reactive oxygen species (ROS) such as superoxide, hydrogen peroxide (H2O2), and hydroxyl radical, can be produced by intracellular aerobic respiration and/or environments. They are toxic to bacterial cells, leading to loss of fitness, including high mutation rates, growth defects, and even cell death. Biochemically, there are two basic classes of H2O2-degrading proteins

1. Catalase: $2H_2O_2 \rightarrow O_2 + 2H_2O$
2. Peroxidases: $RH_2 + H_2O_2 \rightarrow R + 2H_2O$

The electron source of catalase is from H2O2 itself and no exogenous electron source is needed. However, peroxidases can differ in their electron donors (i.e., RH_2), which could be glutathione, thioredoxins, NAD(P)H, cytochrome *c*, dyes and other unknowns.

Catalases rely on iron or manganese so they fall into two categories: heme (an iron-containing compound) calatases and non-heme catalases (or manganese). Catalases with only catalatic activity are called mono-functional catalases, and those with both catalatic activity and peroxidatic activities are referred to as bifunctional catalases or catalase-peroxidases.

Peroxidases also fall into two categories: thiol (i.e., RSH)-based peroxidases (peroxiredoxins; abbr. Prx) and non-thiol peroxidases. All peroxiredoxins contain a conserved cysteine that reacts with H2O2 and forms a disulfide before getting reduced back to free thiol. Depending on the variations in the mechanisms of thiol regeneration, peroxidases can be further classified into four groups: alkylhydroperoxide reductases (AhpCF), thiol glutathione peroxidase (Tpx), bacterioferritin comigratory protein (BCP), and glutathione peroxidase (Gpx).

1 *Escherichia coli*

Most of the following information about *E. coli* antioxidant systems come from a review paper [1]. *E. coli* has at least 9 enzymes that have been proposed to be calatases or peroxidases. The major H2O2 scavenging enzyme is Ahp (alkyl hydroperoxide reductase) [2], which consists of two subunits: the small subunit (AhpC), which reduces organic peroxides to their corresponding alcohols, and the large subunit (AhpF), which is involved in the regeneration of oxidized AhpC. AhpF needs NAD(P)H as an electron donor; therefore, Ahp has limited activity under conditions when reducing power is limited (e.g., nutrient starvation).

E. coli also contains two catalases, HPI (hydroperoxidase I, encoded by *katG*) and HPII (hydroperoxidase II, encoded by *katE*). Despite the key role of Ahp, catalase still has an important role in wild-type cells, because the activity of Ahp is saturated at a low concentration of H2O2 ($< 1\ \mu M$). In contrast, catalases have high Km ($\sim 1\ mM$), and therefore become the predominant scavenger when H2O2 concentrations are high. In contrast to Ahp, catalases can provide protection even in energy-depleted cells.

When the entry rate of H2O2 is high, basal level defense is inadequate and adaptive response is needed. Both Ahp and KatG are transcriptionally induced by the transcriptional regulator, OxyR [3]. A key cysteine residue of the OxyR protein is oxidized by H2O2, triggering conformational change from an inactive form (i.e., reduced state) to an active form (oxidized state). The oxidized OxyR then binds to the promoter regions of many genes on the *oxyR* regulon. Reduced OxyR is regenerated by the glutaredoxin/GSH/Gor system upon return to non-stress conditions.

OxyR positively controls genes for peroxide detoxification, such as catalase and peroxiredoxin (katG, ahpCF), Fe-storage miniferritin (dps), glutaredoxin, thioredoxin and glutathione reductase (grxA, trxC, gor), sulfenic acid oxidoreductase (dsbG), ferric uptake regulator (fur), Fe-S-cluster assembly machinery (sufABCDE), ferrochelatase (hemH), manganese import (mntH) and the small RNA (oxyS) [3]. OxyR negatively regulates its own expression and that of the genes for the ferric ion reductase (fhuF), the outer membrane protein (flu), the mannonate hydrolase (uxuAB) and gluconate permease (gntP) [3]. A comprehensive list of genes in the *oxyR* operon is available here.

Other catalases or peroxidases seem to be dispensible. KatE is induced at the transition from exponential phase to stationary phase by RpoS and its induction is OxyR-independent. Mutation in HPII did not affect the log-phase growth phenotype even in strains lacking HPI and/or Ahp [2]. Other peroxidases seem to play other functions than H2O2-degradation *in vivo*, although their activity has been demonstrated. For

example, the *tpx* mutant did not show any phenotype under aerobic growth, while it is more sensitive to organic hydroperoxides. Deletion of *btuE* (Gpx) also does not create sensitivity to H2O2, while the mutant is more sensitive to paraquat and tellurite.

2 *Pseudomonas aeruginosa*

KatA is the major catalase in *P. aeruginosa* whose expression is constitutively highly in all phases of growth (high basal) but increased upon stationary growth phase and H2O2 treatment [4]. It is highly stable and can be found in the extracellular milieu, which ensures the survival of *P. aeruginosa* cells in its biofilm state. Other typical antioxidant enzymes for the defense against H2O2 challenges include catalases (KatB and KatE) and alkyl hydroperoxide-reducing proteins (AhpB, AhpC, and Ohr). The *katA*, *katB*, *ahpB*, and *ahpCF* genes are positively regulated by OxyR. KatA was also found to be regulated by quorum sensing signals [5] and stringent response [6]. Recently, it was reported that KatE was induced by high temperature and requires the disulfide bond formation system for its activity.

2 Modeling H2O2 diffusion, production and decomposition

1 Model assumptions

The intracellular H2O2 concentration is determined by the balances of three processes: diffusion, production and decomposition (Fig. 1). To develop a model of H2O2 fluxes, the following assumptions are made

1. Intracellular H2O2 is produced at a constant rate;
2. Two H2O2-degrading enzymes, Ahp and KatG, are considered;
3. Ahp becomes saturated at a low concentration of H2O2 (low K_m), while KatG has a high K_m. Therefore, decomposition of H2O2 by Ahp and KatG are modelled using Michaelis-Menten and first-order equation respectively;
4. The total OxyR concentration remains a constant and the equilibrium between oxidized and reduced forms of OxyR can be rapidly reached;
5. Both Ahp and KatG are regulated by the oxidized form of OxyR;
6. Both Ahp and KatG are stable proteins and not actively degraded.

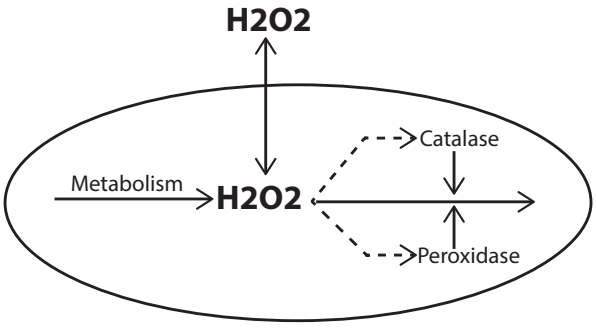

Fig. 1: Schematic diagram of H2O2 reactions. Gene expressions of catalases (KatG) and peroxidases (Ahp) are induced by H2O2 indirectly via oxidation of OxyR.

2 Mathematical equations

Based on the above assumptions, the kinetic equations of intracellular ($[H_i]$) and extracellular ($[H_o]$) H2O2 concentrations are given by

$$\frac{d[H_o]}{dt} = -\frac{([H_o]-[H_i])PA}{V_e} \tag{1}$$

$$\frac{d[H_i]}{dt} = \frac{k_{met}+([H_o]-[H_i])PA}{V_c} - k_{0,cat}[KatG][H_i] - \frac{k_{0,ahp}[Ahp][H_i]}{K_{m,ahp}+[H_i]} \tag{2}$$

where $[KatG]$ and $[Ahp]$ are the concentrations of KatG and Ahp respectively. Parameters include the metabolic production rate of H2O2 (k_{met}), the membrane permeability (P), the surface area of the membrane (A), the cell volume (V_c), the medium volume (V_e), the specific activity of KatG ($k_{0,cat}$), the Ahp's turnover rate ($k_{0,ahp}$), and the half-maximal degradation concentration ($K_{m,ahp}$).

The oxidized ($[OxyR_{ox}]$) and reduced ($[OxyR_{red}]$) forms of OxyR can be interconverted dynamically

$$\mathrm{OxyR_{red}} + \mathrm{n_{oxyr}H_2O_2} \underset{\mathrm{k_{b-}}}{\overset{\mathrm{k_{b+}}}{\longleftrightarrow}} \mathrm{OxyR_{red}(H_2O_2)_{n_{oxyr}}} \xrightarrow{\mathrm{k_{oxyr,ox}}} \mathrm{OxyR_{ox}} \xrightarrow{\mathrm{k_{oxyr,red}}} \mathrm{OxyR_{red}}$$

where k_{b+} and k_{b-} are the forward and reverse binding constants, n_{oxyr} is the stoichiometry of H2O2 molecule in the binding complex between OxyR and H2O2, and $k_{oxyr,ox}$ and $k_{oxyr,red}$ are the rates of OxyR oxidation and reduction respectively. Under the assumption of rapid binding/unbinding equilibrium between $OxyR_{red}$ and H2O2, the chemical kinetics in the equation can be described using differential-algebraic equations

$$\frac{d[OxyR_{ox}]}{dt} = k_{switch}[OxyR_{red}] - k_{oxyr,red}[OxyR_{ox}] \quad (3)$$

$$k_{switch} = \frac{k_{oxyr,ox}[H_i]^{n_{oxyr}}}{K_{m,oxyr}^{n_{oxyr}} + [H_i]^{n_{oxyr}}} \quad (4)$$

$$OxyR_t = [OxyR_{ox}] + [OxyR_{red}] \quad (5)$$

where $K_{m,oxyr}(=(k_{b-}+k_{oxyr,ox})/k_{b+})$ is the dissociation constant and $OxyR_t$ is the total OxyR concentration, which is assumed a constant. If we further assume that the equilibrium between $OxyR_{ox}$ and $OxyR_{red}$ can be rapidly reached and set Eq. 3 to zero, we obtain the fraction of oxidized OxyR at steady state

$$f_{oxyr} = \frac{[OxyR_{ox}]_{ss}}{OxyR_t} = \frac{[H_i]^{n_{oxyr}}}{[H_i]^{n_{oxyr}}\left(1+\frac{k_{oxyr,red}}{k_{oxyr,ox}}\right) + \frac{k_{oxyr,red}}{k_{oxyr,ox}}K_{m,oxyr}^{n_{oxyr}}} \quad (6)$$

Note that the H2O2 concentration (H_{50}) required to oxidize half of the total OxyR ($f_{oxyr}=0.5$) is different from $K_{m,oxyr}$, depending on the ratio between $k_{oxyr,ox}$ and $k_{oxyr,red}$ (we will revisit this point in Sect. 4.1)

$$H_{50} = \left(\frac{k_{oxyr,red}}{k_{oxyr,ox}-k_{oxyr,red}}\right)^{\frac{1}{n_{oxyr}}} K_{m,oxyr} \quad (7)$$

Finally, we assume that the protein synthesis rates of KatG and Ahp are proportional to the fraction of the oxidized OxyR

$$\frac{d[KatG]}{dt} = \alpha_{cat}^{max} f_{oxyr} - \lambda[KatG] \quad (8)$$

$$\frac{d[Ahp]}{dt} = \alpha_{ahp}^{max} f_{oxyr} - \lambda[Ahp] \quad (9)$$

where α_{cat}^{max} and α_{ahp}^{max} are the maximum production rates of KatG and Ahp respectively and λ is the specific growth rate (i.e., the dilution rate).

3 Parameterization

Parameter values are either obtained from literature or estimated by data fitting (see Table 1)

Parameter	Value/Unit	Source
Membrane permeability (P)	$1.6 \times 10^{-3}\ cm/s$	Ref. 7
Membrane area (A)	$1.41 \times 10^{-7}\ cm^2$	Ref. 7
Cytoplasmic volume (V_c)	$3.23 \times 10^{-15}\ L$	Ref. 7
Metabolic production rate of H2O2 (k_{met})	$4.5 \times 10^{-20}\ mol/s$	Ref. 7
Specific enzymatic activity of KatG ($k_{0,cat}$)	$4.188 \times 10^{6}\ (s \cdot M)^{-1}$	Ref. 8
Turnover rate of Ahp ($k_{0,ahp}$)	$52.4\ s^{-1}$	Ref. 9
Maximum protein synthesis rate of KatG (α_{cat}^{max})	$3.62 \times 10^{-24}\ mol/s$	Ref. 10
Maximum protein synthesis rate of Ahp (α_{ahp}^{max})	$1.19 \times 10^{-22}\ mol/s$	Ref. 10
Specific growth rate (λ)	$1.93\ h^{-1}$	Ref. [10]
OxyR-H2O2 dissociation constant ($K_{m,oxyr}$)	$41.32\ \mu M$	Estimated
OxyR-H2O2 binding Hill coefficient (n_{oxyr})	1.36	Estimated
OxyR oxidation rate ($k_{oxyr,ox}$)	$9.99\ s^{-1}$	Estimated
OxyR reduction rate ($k_{oxyr,red}$)	$2.3 \times 10^{-3}\ s^{-1}$	Estimated
Half maximal H2O2 degradation concentration ($K_{m,ahp}$)	$140.61\ nM$	Estimated

Table 1: Parameter values used in the simulations.

Note: α_{cat}^{max} and α_{ahp}^{max} were estimated based on ribosome profiling of exponentially growing *E. coli* cells in MOPS complete medium and λ corresponds to cell growth rate in the same medium. Their values can be underestimated.

4 Results and discussion

4.1 OxyR activation senses both H2O2 concentration and cell redox status

Fig. 2 shows that the H2O2 concentration required to oxidize half of the total OxyR (orange circles; $87.35\ nM$) is much lower than that is required to reach half maximal forward oxidation rate (blue circles; $41.32\ \mu M$). This can be explained by Eq. 7: H_{50} can be much smaller than $K_{m,oxyr}$ under the condition $k_{oxyr,red} \ll k_{oxyr,ox}$. Our estimation shows that $k_{oxyr,red}/k_{oxyr,ox} = 2.3 \times 10^{-4}$. The value of $k_{oxyr,red}$ corresponds to a half life of 5 min, which is consistent with previous observations [11].

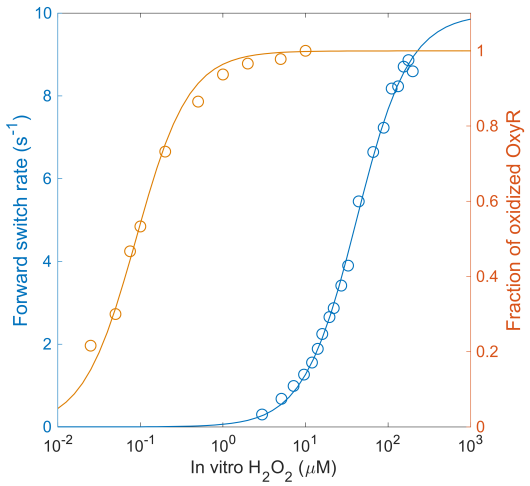

Fig. 2: Eq. 4 and Eq. 6 were fit to experimental data (orange circles [11]; blue circles [12]).

This is interesting because when OxyR proteins are half oxidized, the forward conformational switch rate is only 0.023% of its observed maximum capacity. The reason why the dynamic ranges of the two

responsive curves do not coincide with each other has not been discussed in literature. One possibility is that the oxidation of OxyR is not solely dependent on H2O2 concentration, but also senses the overall redox status. Oxidized OxyR is reduced by the glutaredoxin (GSH) system. Glutathione reductase catalyzes the NADPH-driven reduction of GSSG (the oxidized form of GSH) to GSH; therefore, the GSH recycling is intimately coupled to the balance between NADHP and NADP, which is an indicator of cellular redox state. A drop in the ratio of GSH to GSSG decreases $k_{oxyr,red}$ and consequently activate OxyR regulons to restore redox homeostasis at smaller H2O2 concentration. The huge difference between the H2O2 concentration required to activate conformational switch and required to oxidize OxyR indicates that the cell redox status is low and NADPH may be limiting.

4.2 The relation between intracellular and extracellular H2O2 concentration is threshold-like

Fig. 3 shows that the intracellular H2O2 concentration remains a constant before extracellular H2O2 concentration exceeds a threshold ($\approx 50\ \mu M$). At the maximum buffering capacity, the ratio of extracellular and intracellular H2O2 concentratioin is approximately 100, as shown in the right panel of Fig. 3. Compared to a previous estimate of 10-fold concentration difference [7], our estimation is consistent with additional data that was not considered before (we will revisit this point in Sect. 4.4). When the extracellular H2O2 increases further, the antioxidant system loses its buffering effect and the intracellular and extracellular H2O2 concentrations are roughly equal. This biphasic response has been reported in yeast strain *Saccharomyces pombe* [13], where the H2O2-triggered permanent inactivation of Prx due to hyperoxidation is a key mechanism. However, bacterial 2-Cys Prx, such as the *E. coli* peroxiredoxin AhpC, are much less sensitive to hyperoxidation. Our results show that hyperoxidation is not a necessary component of generating the biphasic response.

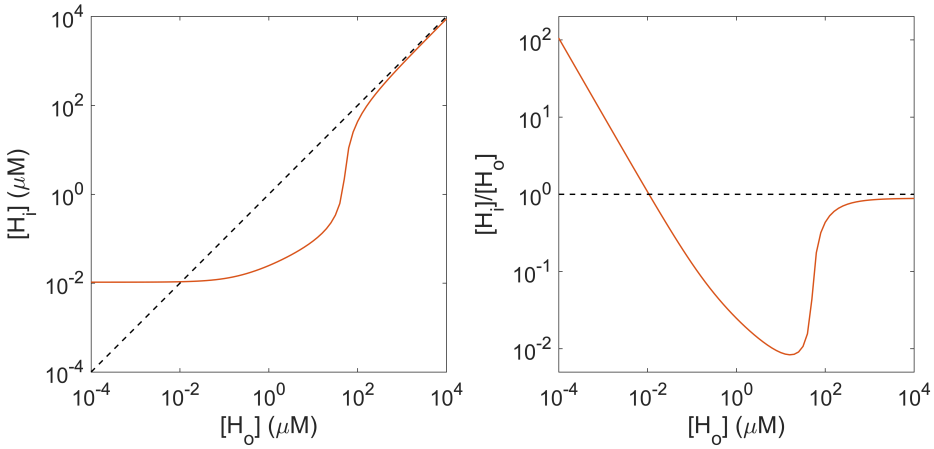

Fig. 3: The absolute intracellular H2O2 concentration (left panel) and relative ratio (right panel) at varied external H2O2 concentration.

4.3 The threshold-behavior is caused by zero-order ultrasensitivity under Ahp saturation

Then it is interesting to understand why the antioxidant system loses its buffering effect suddenly within a narrow range of extracellular H2O2 concentration. To allow analytical analysis, we first simplify the model by assuming constant Cat and Ahp concentrations and define two lumped parameters $k_{cat} = k_{0,cat}[KatG]$ and $k_{ahp} = k_{0,ahp}[Ahp]$. We then rewrite Eq. 2 as follows

$$\frac{dH_i}{dt} = k_{met} + ([H_o] - [H_i])PA - k_{cat}H_i - \frac{k_{ahp}H_i}{K_{m,ahp} + [H_i]} \tag{10}$$

At steady state, we can solve $[H_i]$ as a function of $[H_o]$

$$[H_i] = \frac{-\Delta + \sqrt{\Delta^2 + 4K_{m,ahp}(PA + k_{cat})(k_{met} + [H_o]PA)}}{2(PA + k_{cat})} \tag{11}$$

$$\Delta = K_{m,ahp}PA + K_{m,ahp}k_{cat} - [H_o]PA - k_{met} + k_{ahp} \tag{12}$$

When $K_{m,ahp}$ is a small parameter (i.e., Ahp becomes saturated easily), we can expand Eq. 11 using power series of $K_{m,ahp}$

$$[H_i] = \begin{cases} \dfrac{[H_o]PA + k_{met}}{k_{ahp} - [H_o]PA - k_{met}} K_{m,ahp} + \mathcal{O}(K_{m,ahp}^2) & [H_o] < \dfrac{k_{ahp} - k_{met}}{PA} \\ \dfrac{[H_o]PA + k_{met} - k_{ahp}}{PA + k_{cat}} + \dfrac{k_{ahp}}{[H_o]PA + k_{met} - k_{ahp}} K_{m,ahp} + \mathcal{O}(K_{m,ahp}^2) & [H_o] \geq \dfrac{k_{ahp} - k_{met}}{PA} \end{cases}$$

In the limit of $K_{m,ahp} \to 0$, $[H_i]$ switches abruptly from zero to a non-zero value when $[H_o]$ exceeds $(k_{ahp} - k_{met})/(PA)$. This phenomenon is also called zero-order ultrasensitivity [14] because such ultrasensitive behavior occurs when enzymes operate near saturation.

4.4 The zero-order ultrasensitivity is experimentally confirmed by *in vivo* measurement of oxidized OxyR fraction

If the response of intracellular H2O2 to external H2O2 concentration is indeed ultrasensitive, then this ultrasensitivity must result in the ultrasensitive oxidation of OxyR, i.e., the fraction of oxidized OxyR increases abruptly as well when the extracellular H2O2 concentration exceeds a threshold. Indeed, such ultrasensitivity has been reported by Åslund et al. [11]. Using Åslund's data, Pillay et al. [15] fit a Hill function to the response curve and found that the Hill coefficient is as high as 10.7. By simulating the the steady-state oxidized OxyR fraction at varied extracellular H2O2 concentration (Fig. 4), we showed that decreasing $K_{m,ahp}$ makes OxyR response more and more switch-like.

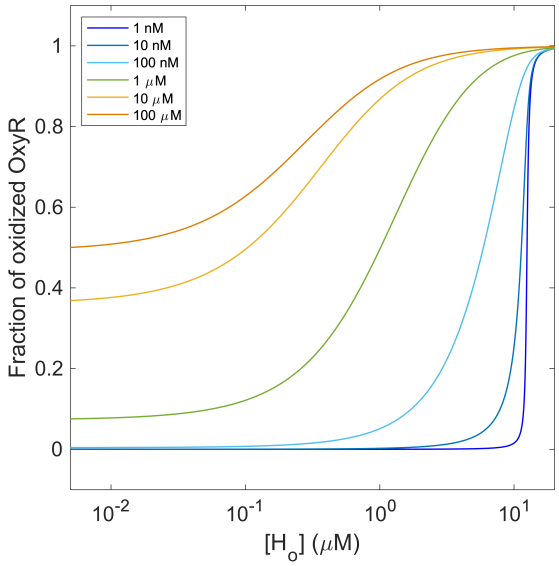

Fig. 4: Decreasing $K_{m,ahp}$ (values given in the legend) increases ultrasensitivity of OxyR oxidation to extracellular H2O2 concentration.

The value of $K_{m,ahp}$ was firstly estimated to be $1.2\ \mu M$ in the paper by Seaver and Imlay [7]. The only dataset they used to estimate $K_{m,ahp}$ was the H2O2 decomposition rate at different extracellular H2O2

concentrations. With the data, they have to estimate the intracellular H2O2 concentration using their model, which may bring errors in the estimation of $K_{m,ahp}$. Since $K_{m,ahp}$ affects the sensitivity of OxyR oxidation, we re-estimated $K_{m,ahp}$ by combining both the H2O2 decomposition data and the OxyR oxidation data. The best-fits of the two datasets are shown in Fig. 5 and the optimal value of $K_{m,ahp}$ is $140.61\ nM$. This value is consistent with previous estimation that an intracellular concentration of about $200\ nM$ is sufficient to drive OxyR into the oxidized form [16].

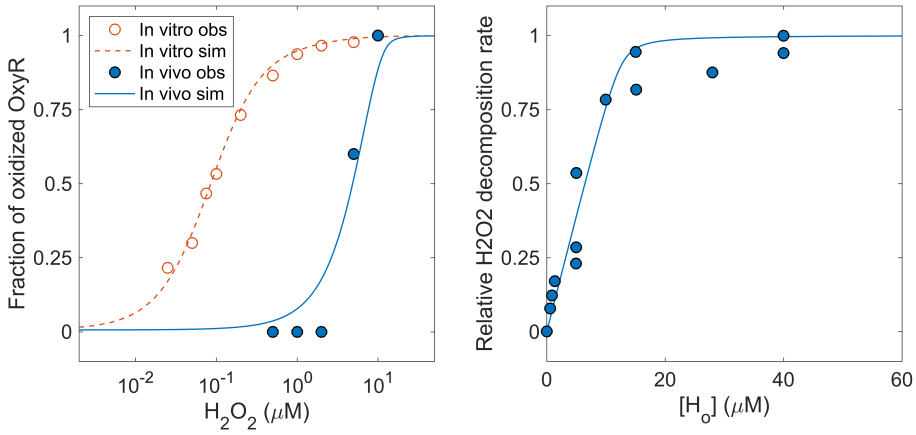

Fig. 5: Fitting $K_{m,ahp}$ to experimental data. Data sources: Left panel [11] and right panel [7]. For the x-axis of the left panel, *in vitro* and *in vivo* indicate the dependence of oxidized OxyR on intracellular and extracellular H2O2 concentrations respectively. The observed and simulated *"in vitro"* data are the same as shown in Fig. 2.

3 References

[1] Surabhi Mishra and James Imlay. Why do bacteria use so many enzymes to scavenge hydrogen peroxide? *Archives of biochemistry and biophysics*, 525(2):145–160, 2012.

[2] Lauren Costa Seaver and James A Imlay. Alkyl hydroperoxide reductase is the primary scavenger of endogenous hydrogen peroxide in escherichia coli. *Journal of bacteriology*, 183(24):7173–7181, 2001.

[3] Melanie Hillion and Haike Antelmann. Thiol-based redox switches in prokaryotes. *Biological chemistry*, 396(5):415–444, 2015.

[4] Yun-Jeong Heo, In-Young Chung, Wan-Je Cho, Bo-Young Lee, Jung-Hoon Kim, Kyoung-Hee Choi, Jin-Won Lee, Daniel J Hassett, and You-Hee Cho. The major catalase gene (kata) of pseudomonas aeruginosa pa14 is under both positive and negative control of the global transactivator oxyr in response to hydrogen peroxide. *Journal of bacteriology*, 192(2):381–390, 2010.

[5] Daniel J Hassett, Ju-Fang Ma, James G Elkins, Timothy R McDermott, Urs A Ochsner, Susan EH West, Ching-Tsan Huang, Jessie Fredericks, Scott Burnett, Philip S Stewart, et al. Quorum sensing in pseudomonas aeruginosa controls expression of catalase and superoxide dismutase genes and mediates biofilm susceptibility to hydrogen peroxide. *Molecular microbiology*, 34(5):1082–1093, 1999.

[6] Malika Khakimova, Heather G Ahlgren, Joe J Harrison, Ann M English, and Dao Nguyen. The stringent response controls catalases in pseudomonas aeruginosa: Implications for hydrogen peroxide and antibiotic tolerance. *Journal of bacteriology*, pages JB–02061, 2013.

[7] Lauren Costa Seaver and James A Imlay. Hydrogen peroxide fluxes and compartmentalization inside growing escherichia coli. *Journal of bacteriology*, 183(24):7182–7189, 2001.

[8] Al Claiborne and I Fridovich. Purification of the o-dianisidine peroxidase from escherichia coli b. physicochemical characterization and analysis of its dual catalatic and peroxidatic activities. *Journal of Biological Chemistry*, 254(10):4245–4252, 1979.

[9] Derek Parsonage, P Andrew Karplus, and Leslie B Poole. Substrate specificity and redox potential of ahpc, a bacterial peroxiredoxin. *Proceedings of the National Academy of Sciences*, 105(24):8209–8214, 2008.

[10] Gene-Wei Li, David Burkhardt, Carol Gross, and Jonathan S Weissman. Quantifying absolute protein synthesis rates reveals principles underlying allocation of cellular resources. *Cell*, 157(3):624–635, 2014.

[11] Fredrik Åslund, Ming Zheng, Jon Beckwith, and Gisela Storz. Regulation of the oxyr transcription factor by hydrogen peroxide and the cellular thiol—disulfide status. *Proceedings of the National Academy of Sciences*, 96(11):6161–6165, 1999.

[12] Cheolju Lee, Soon Mi Lee, Partha Mukhopadhyay, Seung Jun Kim, Sang Chul Lee, Woo-Sung Ahn, Myeong-Hee Yu, Gisela Storz, and Seong Eon Ryu. Redox regulation of oxyr requires specific disulfide bond formation involving a rapid kinetic reaction path. *Nature Structural and Molecular Biology*, 11(12):1179, 2004.

[13] Lewis Elwood Tomalin, Alison Michelle Day, Zoe Elizabeth Underwood, Graham Robert Smith, Piero Dalle Pezze, Charalampos Rallis, Waseema Patel, Bryan Craig Dickinson, Jürg Bähler, Thomas Francis Brewer, et al. Increasing extracellular h2o2 produces a bi-phasic response in intracellular h2o2, with peroxiredoxin hyperoxidation only triggered once the cellular h2o2-buffering capacity is overwhelmed. *Free Radical Biology and Medicine*, 95:333–348, 2016.

[14] James E Ferrell Jr and Sang Hoon Ha. Ultrasensitivity part i: Michaelian responses and zero-order ultrasensitivity. *Trends in biochemical sciences*, 39(10):496–503, 2014.

[15] Ché S Pillay, Beatrice D Eagling, Scott RE Driscoll, and Johann M Rohwer. Quantitative measures for redox signaling. *Free Radical Biology and Medicine*, 96:290–303, 2016.

[16] James A Imlay. The molecular mechanisms and physiological consequences of oxidative stress: lessons from a model bacterium. *Nature Reviews Microbiology*, 11(7):443, 2013.